LA-UR-17-22600
Approved for public release; distribution is unlimited.

Title: Limited Range Sesame EOS for Ta

Author(s): Greeff, Carl William
Crockett, Scott
Rudin, Sven Peter
Burakovsky, Leonid

Intended for: Report

Issued: 2017-03-30

Limited Range Sesame EOS for Ta

C. W. Greeff, S. D. Crockett, L. Burakovsky, and S. P. Rudin (T-1)
Los Alamos National Laboratory, Los Alamos, NM 87545
(Dated: Feb. 14 2017)

A new Sesame EOS table for Ta has been released for testing. It is a limited range table covering $T \leq 26,000$ K and $\rho \leq 37.53$ g/cc. The EOS is based on earlier analysis using DFT phonon calculations to infer the cold pressure from the Hugoniot. The cold curve has been extended into compression using new DFT calculations. The present EOS covers expansion into the gas phase. It is a multi-phase EOS with distinct liquid and solid phases. A cold shear modulus table (431) is included. This is based on an analytic interpolation of DFT calculations.

I. INTRODUCTION

A new Sesame equation of state table for Tantalum has been created and released for testing. The material ID is 93524. The 9 will be dropped when the EOS has undergone sufficient testing. This table builds on earlier work [1] which used shock and ambient pressure data together with density functional theory (DFT) calculations of phonon frequencies to infer the static lattice pressure. That earlier work used a special form for the electron-thermal contribution to the EOS which was not suitable for extrapolation to low or high density, or high temperature. The present table uses the Thomas Fermi Dirac (TFD) model, which covers the full range.

The table covers temperatures $T \leq 26,000$ K and densities $\rho \leq 37.53$ g/cc. It is a multi-phase EOS [2], with the liquid and (bcc) solid treated as distinct phases, and coexistence regions are tabulated. A table giving the cold shear modulus as a functions of density (431 table) is included. The data are based on an analytic interpolation of DFT calculations.

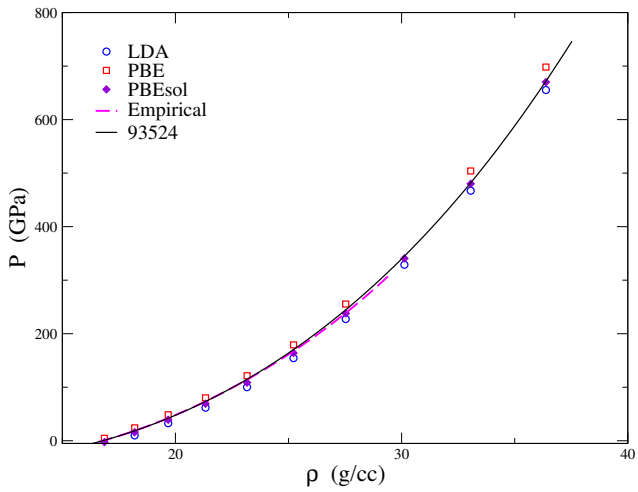

FIG. 1: Ta static lattice pressure. Solid black curve is present EOS. Dashed magenta curve is our semi-empirical analysis from ref. [1]. Symbols are DFT calculations with various approximate exchange-correlation functionals.

II. EOS MODEL

The Helmholtz free energy for each phase is written as

$$F_i(V,T) = \phi_i(V) + F_i^{\rm ion}(V,T) + F_i^{\rm el}(V,T) \qquad (1)$$

where ϕ is the static lattice energy, $F^{\rm ion}$ is the ion motion contribution, and $F^{\rm el}$ is the electronic excitation term. The subscript i denotes the phase. In the present model, two phases, the bcc solid, and the liquid, are considered explicitly. We have produced an equilibrium table. It includes mixed phase regions in which,

$$\begin{aligned} P_l(V_l,T) &= P_s(V_s,T) \\ G_l(V_l,T) &= G_s(V_s,T) \\ \lambda_l V_l + \lambda_s V_s &= V \\ \lambda_l E_l(V_l,T) + \lambda_s E_s(V_s,T) &= E \end{aligned} \qquad (2)$$

where P, G, V, and E denote the pressure, specific Gibbs free energy, volume, and internal energy, respectively, and λ_i denotes the mass fraction of phase i. For the great majority of states, there are no solutions to the conditions 2 satisfying $0 \leq \lambda_i \leq 1$ and $\sum_i \lambda_i = 1$, and the state is a pure phase with the lowest Helmholtz free energy at the given V and T. The algorithm for constructing equilibrium tables is described in ref. [2].

Our model parameters are based on an earlier analysis [1]. There we used DFT calculations of phonon frequencies and the electronic density of states to determine the ion and electronic free energies, and inferred an empirical static lattice pressure based on ambient pressure lattice parameter and bulk modulus together with solid phase shock Hugoniot data. In the present case, we wish to extend the EOS to higher compression and also down to gas phase densities. The electronic model used in ref. [1] used a functional form that was not suitable for extrapolation in density or temperature. Here we have used the TFD model instead, which does not contain as much detail, but is applicable over a wide range.

Our earlier analysis gave ϕ to about 29.5 g/cc, the density of the highest solid phase Hugoniot point. To extend beyond this, we performed DFT calculations using various approximations for the exchange-correlation

functional. As is typical, we found that the LDA functional underestimates the pressures and the PBE functional overestimates them. The more recent PBEsol [3] and AM05 [4] functionals give similar results with small errors compared to the empirical static lattice pressure. The PBEsol functional converged more reliably in the Elk LAPW code [5], which we used for these calculations, so we have extended our empirical static lattice pressure using calculations with the PBEsol functional. This is illustrated in figure 1.

The electronic free energy is the TFD model for both solid an liquid phases. The ion model for the solid phase is the Debye model. The volume dependence of the Debye temperature is the same as was determined in ref. [1] using DFT phonon calculations. These calculations gave a density-dependent Grüneisen parameter, γ, with $\gamma(\rho_{\rm ref}) = 1.61$, where $\gamma = d\ln\theta/d\ln\rho$ and $q = -d\ln\gamma/d\ln\rho = 0.2824$. The ion model for the liquid is the high-T liquid model described in [6]. This model is Debye-like at low T, has a specific heat that falls from $3k$/atom to $\frac{3}{2}k$/atom at intermediate temperatures, with the free energy merging into that of an ideal gas at very high T. There is a Grüneisen parameter that enters into the Debye-like free energy, and also controls the temperature scale for the decay of the specific heat. This is taken to be the same as that of the bcc solid. In addition, the liquid has a constant entropy offset ΔS_V with respect to a Debye-like solid, which was determined to be $\Delta S_V = 1k$/atom using ambient pressure data. The liquid has a density-dependent energy offset $\Delta\phi(\rho) = \Delta S_V T_m(\rho)$, where T_m is the melting temperature. The function $T_m(\rho)$ is described by its own Grüneisen parameter,

$$\frac{d\ln T_m}{d\ln\rho} = 2\gamma_m - \frac{2}{3}. \qquad (3)$$

For Lindemann melting, γ_m is the same as the Debye Grüneisen parameter of the solid. In order to get the correct shock melting pressure of ~ 300 GPa, we reduced $\gamma_m(\rho_{\rm ref})$ from 1.61 to 1.4, lowering the melting curve.

Figure 2 shows the Hugoniot in the shock velocity, U_S, particle velocity U_p plane, along with data from various sources [7–11]. The data from Mitchell and Nellis [11] were especially weighted in our earlier analysis [1] and in the present work because of their small error bars, which are similar to the size of the plotting symbols in the figure.

Figure 3 shows the Hugoniot and room temperature isotherm in the pressure-density plane. The Hugoniot data is as described above. The room temperature data is from [12–14]. The Hugoniot lies in the solid phase below 305 GPa. Between 305 and 377 GPa, the shocked states are mixed solid and liquid, and above 377 GPa, the Hugoniot lies in pure liquid. These melting effects are subtle, but distinguishable as small discontinuities of the slope of the $P(\rho)$ Hugoniot curve.

The room temperature data were not used as inputs to this EOS. The static lattice pressure was based on

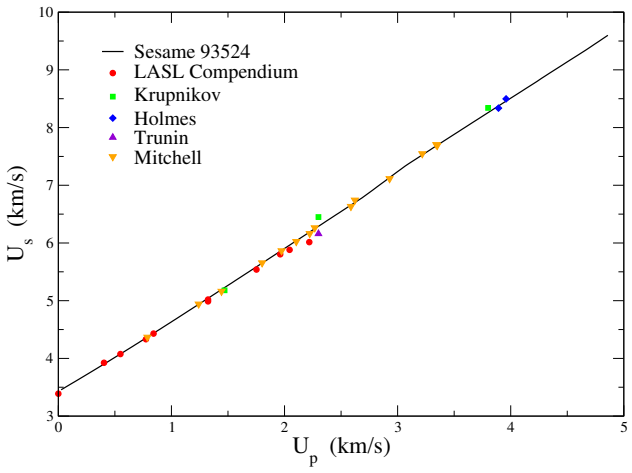

FIG. 2: Ta Hugoniot. Solid black curve is present EOS. Data from [7–11]

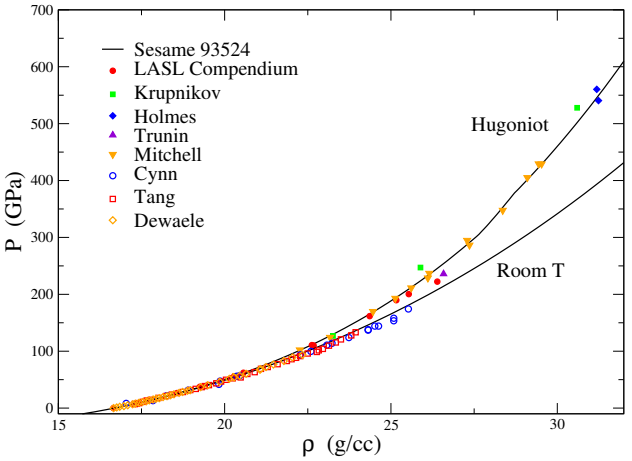

FIG. 3: Hugoniot and room temperature isotherm of Ta. Hugoniot data are as in figure 2. Room temperature data are from [12–14].

the Hugoniot data and DFT calculations, and the room temperature isotherm was inferred. There is generally good agreement with the data to ~ 90 GPa. Above this, both the Cynn and Yoo [12] and Tang *et al.* [14] give systematically lower pressures than the current EOS. Figure 4 shows a more detailed view of the room temperature isotherm below 200 GPa. The data from Tang *et al.* [14] uses the calibration of the ruby pressure scale of Mao *et al.* [15]. This calibration was originally developed for pressures below 80 GPa, and has since been extrapolated higher. There is now a general consensus that the 1986 Mao *et al.* ruby scale gives pressures that are too low when extrapolated this way [16]. We have re-evaluated

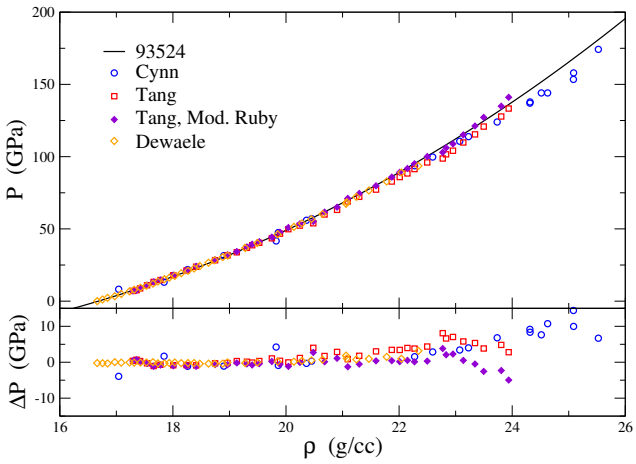

FIG. 4: Room temperature isotherm of Ta. The data from Tang *et al.* [14] uses the calibration of the ruby pressure scale of Mao *et al.* [15]. The solid violet diamonds show the result of applying the more recent ruby pressure scale [13] to the Tang *et al.* data. The lower graph shows the difference of the present EOS, 93524 from the various data sources.

the pressures from Tang *et al.* using the modified ruby scale of Dewaele *et al.* [13]. These pressures are shown as the filled violet diamonds in figure 4. These data are in good agreement with our EOS to ~ 100 GPa, as are the data from Dewaele *et al.* [13]. At higher pressures the data become scattered, with the Cynn and Yoo data lying below our EOS and the corrected Tang *et al.* data above it.

The Lennard-Jones match procedure[17] has been used for $\phi(\rho)$ for $\rho < 0.98\rho_{\rm ref}$. The cohesive energy has been adjusted to match vapor pressure data [18]. The boiling point that results is 5736 K. The critical point parameters are,

$$\begin{aligned} T_c &= 16200\text{K} \\ P_c &= 1.9\text{GPa} \\ \rho_c &= 4.57 g/cc\,. \end{aligned} \tag{4}$$

Estimated critical temperatures for Ta cover a wide range, from 9284 to 17329 K [19].

III. SHEAR MODULUS

The EOS table includes a cold shear modulus table (431 table). This is based on the functional form [20],

$$G = G_{\rm ref}\left(\frac{\rho}{\rho_{\rm ref}}\right)^{1/3} \exp\left[6g_1\left(\rho_{\rm ref}^{-1/3}-\rho^{-1/3}\right) + 2\frac{g_2}{q}\left(\rho_{\rm ref}^{-q}-\rho^{-q}\right)\right] \tag{5}$$

The parameters are

$$\begin{aligned} G_{\rm ref} &= 72.2 \\ \rho_{\rm ref} &= 16.68 \\ g_1 &= 3.0567 \\ g_2 &= -6.6 \\ q &= 1.0 \end{aligned} \tag{6}$$

where the units are GPa for G and g/cc for ρ. These parameters are fitted to DFT calculations of $G(\rho)$. Expression 5 is meant to be used in compression. The table is required to cover all densities. For densities below $\rho = \frac{1}{2}\rho_{\rm ref}$, we have augmented Eq. 5 with an extension that is continuous, has continuous first derivative and goes to zero as $\exp(-c/\rho)$.

[1] C. W. Greeff, S. P. Rudin, S. Crockett, and J. M. Wills, in *AIP Conference Proceedings*, edited by M. Elert, M. D. Furnish, W. W. Anderson, W. G. Proud, and W. T. Butler (AIP, 2009), vol. 1195, pp. 681–684.

[2] C. Greeff, E. Chisolm, and D. George, Los Alamos National Laboratory Tech. Rep. No. LA-UR-05-9414 (2005).

[3] J. P. Perdew, A. Ruzsinszky, G. I. Csonka, O. A. Vydrov, G. E. Scuseria, L. A. Constantin, X. Zhou, and K. Burke, Phys. Rev. Lett. **100**, 136406 (2008), URL `http://link.aps.org/doi/10.1103/PhysRevLett.100.136406`.

[4] R. Armiento and A. E. Mattsson, Phys. Rev. B **72**, 085108 (2005), URL `http://link.aps.org/doi/10.1103/PhysRevB.72.085108`.

[5] K. Dewhurst, *The elk fp-lapw code*, http://elk.sourceforge.net.

[6] E. D. Chisolm and D. C. Wallace, Los Alamos National Laboratory Tech. Rept. LA-UR-04-3948 (2004).

[7] S. P. Marsh, *LASL Shock Hugoniot Data* (University of California Press, Berkeley, CA, 1980).

[8] K. K. Krupnikov, A. A. Bakanova, R. F. Trunin, and M. I. Brazhnik, Doklady Akademii Nauk SSSR **148**, 1302 (1963), ISSN 0002-3264.

[9] N. C. Holmes, J. A. Moriarty, G. R. Gathers, and W. J. Nellis, Journal of Applied Physics **66**, 2962 (1989), URL `http://dx.doi.org/10.1063/1.344177`.

[10] R. F. Trunin, L.F.Gudarenko, M. V. Zhernokletov, and G. V. Simakov, RFNC, Sarov (2001).

[11] A. C. Mitchell and W. J. Nellis, Journal of Applied Physics **52**, 3363 (1981), http://dx.doi.org/10.1063/1.329160, URL `http://dx.doi.org/10.1063/1.329160`.

[12] H. Cynn and C.-S. Yoo, Phys. Rev. B **59**, 8526 (1999), URL `http://link.aps.org/doi/10.1103/PhysRevB.59.8526`.

[13] A. Dewaele, P. Loubeyre, and M. Mezouar, Phys. Rev. B **70**, 094112 (2004), URL `http://link.aps.org/doi/10.1103/PhysRevB.70.094112`.

[14] L.-Y. Tang, L. Liu, J. Liu, W.-S. Xiao, Y.-C. Li, X.-

D. Li, and Y. Bi, Chinese Physics Letters **27**, 016402 (2010), URL http://stacks.iop.org/0256-307X/27/i=1/a=016402.

[15] H. K. Mao, J. Xu, and P. M. Bell, Journal of Geophysical Research: Solid Earth **91**, 4673 (1986), ISSN 2156-2202, URL http://dx.doi.org/10.1029/JB091iB05p04673.

[16] P. I. Dorogokupets and A. R. Oganov, Phys. Rev. B **75**, 024115 (2007), URL http://link.aps.org/doi/10.1103/PhysRevB.75.024115.

[17] J. Abdallah, Tech. Rep. LA-10244-M, Los Alamos National Laboratory (1984).

[18] R. Hultgren, P. D. Desai, D. T. Hawkins, M. Gleiser, and K. K. Kelley, Tech. Rep., DTIC Document (1973).

[19] A. Ray, M. Srivastava, G. Kondayya, and S. Menon, Laser and Particle Beams **24**, 437 (2006).

[20] L. Burakovsky, C. W. Greeff, and D. L. Preston, Physical Review B **67**, 094107 (2003).